Wafer-Level Packaging Based on Uniquely Orienting Self-Assembly (The DUO-SPASS Processes)

Jiandong Fang and Karl F. Böhringer, *Senior Member, IEEE*

***Abstract*—A wafer-level packaging strategy for micro device chips based on uniquely orienting self-assembly is presented with the following steps: 1) bulk parts are uniquely face-oriented and spread in a single layer; 2) parts are palletized onto an alignment template having an array of receptor sites; 3) parts are anchored one-to-one to the receptor sites; 4) each anchored part is fixed to a unique in-plane orientation. We demonstrate all of these steps with two different self-organizing parallel assembly (SPASS) processes: a semidry uniquely orienting process (semi-DUO-SPASS) and a dry uniquely orienting (DUO-SPASS) process. The semidry process exploits: 1) an agitated air/water interface to uniquely face-orient bulk parts having a single hydrophobic face; 2) a hydrophobic carrier wafer to palletize the parts in an air environment; 3) orbital shaking to drive the parts until they are anchored to receptor sites; 4) gravity to uniquely align the parts. Experiments show that 2-mm square silicon parts are correctly registered on a 4-in alignment template having 164 receptor sites with a defect rate of $\sim 1\%$ after 3 min orbital shaking. The dry process utilizes: 1) asymmetry in dynamic stability to uniquely face-orient bulk parts having protruding features on one face; 2) orbital shaking to drive the parts until they are first anchored to receptor sites and then fixed in well-defined in-plane orientations by two-stage shape recognition. In our experiments, 1-mm square silicon parts are assembled with a defect rate of $\sim 2\%$ in 10 min on each of two 4-in alignment templates having, respectively, 397 and 720 receptor sites. [1490]**

***Index Terms*—Self-organizing parallel assembly (SPASS) process, two-stage shape recognition, uniquely orienting self-assembly, wafer-level packaging.**

I. Introduction

MICRO assembly is required in both packaging of micro device chips and integration of complex hybrid micro systems. Current micro assembly technologies can be categorized as: micromanipulator based assembly [1]–[7], wafer-to-wafer devices transfer [8]–[11], fluidic shape-directed self-assembly [12], [13], and capillary-driven self-assembly [14]–[16]. Each of these assembly techniques has its limitations: micromanipulator-based assembly processes are serial and slow, and micro parts tend to stick to micromanipulators because adhesive forces dominate gravitational forces; wafer-to-wafer pattern transfer is limited to microstructures fabricated on the same substrate; most types of microchips have rectangular shapes due to mechanical dicing along straight lines, but neither fluidic shape-directed self-assembly nor capillary-driven self-assembly can align them to unique in-plane orientations, which is required, for example, for a microchip with multiple interconnect pads so that correct electrical connections can be achieved via flip-chip bonding [17], [18] to a carrier substrate.

Many methods to orient flat parts have been developed for part feeders of robotic assembly systems. Vibratory bowl methods [19] pick parts with desired orientations via track filters. Programmable squeezing fields [20] uniquely orient some types of flat polygonal parts. Neither of these two methods can uniquely orient parts with rotationally symmetrical shapes. Usually visual feedback systems are used for flexible part feeders ("flexible" means that multiple types of parts can be handled by a single feeder) to present parts with correct orientations [21]. But all these part feeding methods are serial processes and not suitable to handle very large numbers of parts, e.g., for mass packaging of radio frequency identification (RFID) chips.

Uniquely orienting assembly is the key requirement to package micro device chips having multiple interconnect pads. Here we demonstrate two different processes satisfying this requirement: a semidry process based on gravity driven self-alignment and a dry process based on two-stage shape recognition between complementary features on parts and receptor sites.

II. Wafer-Level Packaging Strategy

Usually bulk microdevice chips having multiple interconnect pads on one face ("bonding face") are stored in a container with random face orientations. To package these chips at the wafer level, we propose the following process steps (Fig. 1): 1) bulk parts are oriented to face the same direction with their bonding faces and spread in a single layer; 2) parts are palletized onto an alignment template (AT) with the face orientation preserved; 3) parts are distributed and anchored to receptor sites in a one-to-one mode; 4) parts are uniquely aligned on the receptor sites; 5) aligned parts are transferred to a chip carrier template (CCT) via wafer-level flip-chip bonding. This packaging strategy except step 5, a well-established process in the IC industry, is demonstrated in each of the following two types of self-organizing parallel assembly processes (SPASS): the semidry uniquely orienting process (semi-DUO-SPASS) and the dry uniquely orienting process (DUO-SPASS).

Manuscript received January 1, 2005; revised November 7, 2005. This work was supported in part by the NIH Center of Excellence in Genomic Science and Technology by Grant 1-P50-HG002360-01 and DARPA DSO award FAA9550-04-0257, and by the U.S. Department of Justice Award 2000-DT-CX-K001. The work of K. F. Böhringer was supported in part by a long-term invitational fellowship from the Japanese Society for the Promotion of Science (JSPS). Subject Editor T. Kenny.

The authors are with the Department of Electrical Engineering, University of Washington, Seattle, WA 98195 USA (e-mail: jdfang@ee.washington.edu; karl@ee.washington.edu).

Digital Object Identifier 10.1109/JMEMS.2006.876790

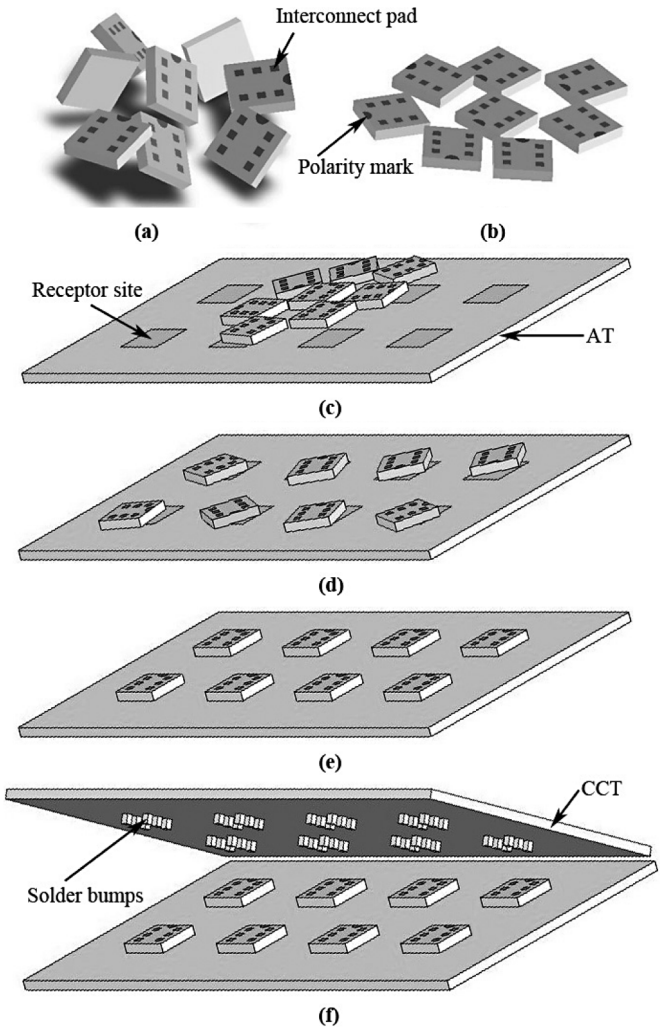

Fig. 1. Wafer-level packaging strategy. (a) Randomly oriented bulk parts. (b) Bulk parts are uniquely face-oriented and spread in a single layer. (c) Parts palletized onto an AT. (d) Parts are distributed one-to-one to receptor sites. (e) Parts are aligned to the receptor sites with unique in-plane orientations. (f) Parts are bonded to a CCT via wafer-level flip-chip bonding.

III. The Semidry Assembly Process (Semi-DUO-SPASS)

This process consisted of two wet steps and two dry steps: bulk parts having only one hydrophobic face (used as a bonding face) were uniquely oriented with their hydrophobic faces upward on an agitated water surface, and stayed together in a single layer; a hydrophobic substrate picked up the floating parts and transferred them onto an alignment template; orbital shaking moved the parts randomly across the alignment template until they were anchored to the receptor sites; anchored parts roughly self-aligned to the receptor sites on an appropriately tilted alignment template to minimize their potential energies. The accuracy of the coarse alignment was greatly improved by capillary-driven self-alignment when appropriate amount of steam condensate was introduced onto the parts.

A. Design Rule for Features on Parts and Receptor Sites

The semidry assembly process is based on the peg-in-hole mechanism: the part has a circular peg (CP) offset from the center of mass, and the receptor site has a circular trench (CT) with a greater diameter than the circular peg. The larger trench

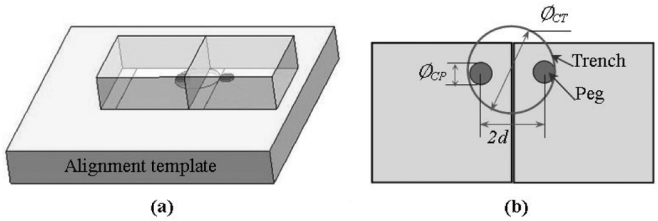

Fig. 2. One-to-one registration design rule. (a) Two parts competing for one receptor site. (b) Top view of the parts and receptor site.

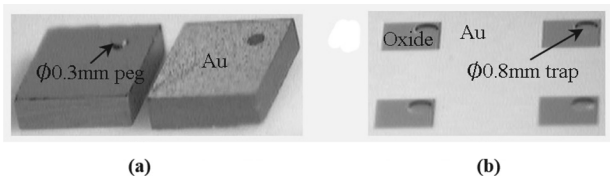

Fig. 3. Microscope images of parts and receptor sites. (a) Top and bottom views of 2-mm square silicon parts. (b) A 2×2 section of an array of 2-mm square receptor sites on a 4-in alignment template.

is used for faster trapping of the peg, i.e., anchoring of a part. For one-to-one registration of parts, the trench diameter must stay below an upper limit $\varnothing_{\mathrm{CT}}$ which is determined by

$$\varnothing_{\mathrm{CT}} = \varnothing_{\mathrm{CP}} + 2d \tag{1}$$

where $\varnothing_{\mathrm{CP}}$ is the diameter of the peg, and d is the smallest distance from the peg center to the part edge (Fig. 2). If this condition is satisfied, no more than one peg can be trapped simultaneously in one trench.

B. Fabrication of Parts and AT

1) Parts: Square diced silicon parts ($\mathrm{side\ length} = 2$ mm) were used to demonstrate the semidry assembly process. We fabricated the parts from a 4-in single side polished (SSP) silicon wafer with the following steps: (1) spincoat photoresist AZ4620 on the polished side and lithographically pattern AZ4620 to cover only circular peg areas ($\varnothing 0.3$ mm); (2) deep reactive ion etch (DRIE) the polished side for about 20 min to form the protruding pegs with 45-μm height; (3) spincoat photoresist AZ1512 on the rough side and lithographically pattern AZ1512 using double side alignment (ABM IR aligner) to cover the circular areas directly opposite to the pegs; (4) sputter deposit a layer of TiW/Au (50/800 Å) on the rough side; (5) strip all the photoresist together with TiW/Au on it in acetone, then rinse the wafer in IPA and DI water, and dry it with a $\mathrm{N_2}$ gun. Finally, the silicon wafer was mechanically diced into 2-mm square parts [Fig. 3(a)]. The opening in the gold layer marks the position of the peg on the other side, as well as the part polarity.

2) Alignment Template: An alignment template with an array of 168 receptor sites was fabricated from a 4-in oxidized SSP silicon wafer (thermal oxide thickness is about 3900 Å) with a DRIE process and a lift-off process. Patterning of the receptor sites on the polished wafer surface was accomplished with the following steps: (1) spincoat AZ4620 and lithographically pattern it to expose only the circular trench areas ($\varnothing 0.8$ mm), then completely remove the exposed oxide in a buffered oxide etchant (BOE) with an etching rate of about

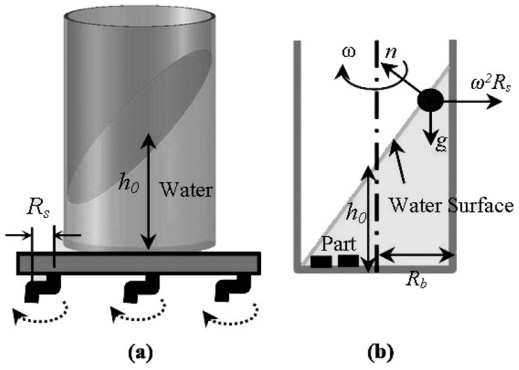

Fig. 4. Schematic view of orbital shaken water surface. (a) Tilted water surface plane. (b) Cross-section view perpendicular to the tilted water surface.

600 Å/min; (2) DRIE the wafer for 20 min to form 60 μm deep trenches (this etching rate is greater than that for the pegs because of the loading effect [22] in the DRIE process), and then strip AZ4620; (3) spincoat AZ1512 and pattern it to cover only square receptor site areas and sputter deposit 50/800 Å TiW/Au; (4) strip AZ1512 and lift off metal in acetone. An array of receptor sites is shown in Fig. 3(b).

3) Surface Treatment: Surface treatment was applied to the silicon parts and the alignment template to prepare them for the assembly process. First, the parts and the template were soaked in a Nano-strip solution (Rockwood Electronic Materials, CA) for half an hour, and then rinsed with DI water. The Nano-strip solution oxidized the silicon surfaces and removed photoresist residues from the gold surfaces. Second, the parts and the template were soaked in a 1-mmol alkanethiol $CH_3(CH_2)_{11}SH$ (in ethanol) solution overnight. The gold surfaces became hydrophobic after adsorbing a self-assembled monolayer (SAM) from the alkanethiol solution. Then each silicon part had only one hydrophobic thiolated gold face, and all the other faces were hydrophilic silicon oxide. The receptor site area was hydrophilic silicon oxide, and its background was a hydrophobic thiolated gold surface. Finally, the parts and the alignment template were dried, respectively, with heating on a 120 °C hotplate and blowing N_2.

C. Uniquely Face-Orienting Bulk Parts

1) Orbital Shaken Water Surface: Water in a stationary glass beaker has a horizontal plane surface when neglecting the slight bending near the hydrophilic beaker sidewall. When the beaker is attached onto a running orbital shaker, the water surface becomes a tilted plane [Fig. 4(a)]. The slope of the tilted plane is determined by the shaking speed, which can be calculated by the following approximate physical model.

Considering a finite element at the tilted water surface, it has three forces [Fig. 4(b)]: gravity (downwards), centrifugal force (horizontal), and supporting force by the nearby water (normal to water surface). The vector sum of these forces goes to zero at a steady state, which indicates that the slope s of the water surface is determined by

$$s = \frac{\omega^2 R_s}{g} \tag{2}$$

where ω is the shaking speed, R_s is the shaker arm length, and g is the gravitational constant.

When neglecting the dragging force from the beaker sidewall, the orbital shaken water surface is still a plane, because both the centrifugal force and gravity are uniform across the water surface, and so is the slope s. The water surface plane is always perpendicular to the vector sum of gravity and centrifugal force.

2) The Face-Orienting Process: Initially bulk parts were randomly oriented, and we invented the following new agitating process to orient all the parts to face the same direction with their pegs before palletizing. The 2-mm square silicon parts can float on a water surface because surface tension is sufficient to balance their gravitational forces. For a smaller part with side length L and thickness t, surface tension ($\propto L$) is even more significant compared with the gravitational force ($\propto L^2 \times t$). We put the 2–mm square silicon parts in a beaker and submerged them with water, and then shook the beaker on an orbital shaker (Model 513500, Cole-Parmer) to tilt the water surface above a speed of ω_c so that some parts were exposed to air. According to (2) and Fig. 4(b), we can calculate this critical shaking speed

$$\omega_c = \sqrt{\frac{h_0 g}{R_b R_s}} \tag{3}$$

where h_0 is the still water level and R_b is the radius of the beaker bottom. In our experiment, these parameters were: $h_0 = 12$, $R_s = 12.7$, and $R_b = 12$ mm. The theoretical and experimental values of ω_c were, respectively, 268 and 310 rpm, and the difference came from the assumption of neglecting friction from the beaker sidewall for the above approximate physical model. Water surface tension dragged and floated the exposed parts. After 1 min shaking, most of the submerged parts floated, and all floating parts had their hydrophobic thiolated gold faces upwards (the only stable state on an agitated water surface) and stayed together in a single layer to minimize potential and interfacial energies.

D. Palletizing Floating Parts

1) Carrier Wafer: A carrier wafer (CW) was used to pick up the floating parts and palletize them onto an alignment template. The carrier wafer was a 3-in pyrex wafer coated with hydrophobic fluorocarbon polymer PFC802 (Cytonix Corp., MD) on one side. When the carrier wafer was inserted into the water vertically, the water surface bent downwards near the hydrophobic PFC802 surface and bent upwards near the hydrophilic pyrex surface (Fig. 5). The contact angle of water on a PFC802 surface is $\theta_c = 110°$. The intersection angle α [Fig. 6(a)] between the carrier wafer and the water surface should be greater than $180° - \theta_c = 70°$ so that the water surface bends downward near the PFC802 surface, and the water valley near the PFC802 surface attracts nearby floating parts by minimizing their potential energies. If α is less than 70°, then the water surface bends upward near the PFC802 surface and the carrier wafer repels nearby floating parts.

2) The Palletizing Process: When the carrier wafer continuously entered the water vertically ($\alpha > 70°$), the parts adhered to the carrier wafer firmly [Fig. 6(a)] due to significant capillary

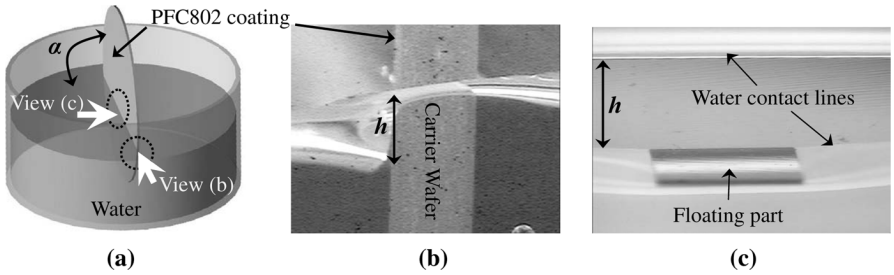

Fig. 5. Water surface bending near CW surfaces. (a) Schematic view of a carrier wafer inserted vertically in water. (b) Side view of water surface bending near both sides of the carrier wafer. (c) Front view of water surface bending near carrier wafer surfaces, and a floating part trapped in the water valley close to the hydrophobic PFC802 surface (the variations in the top surface color of the part is due to lighting effects, in reality, the top surface is uniformly covered with gold except a small mark hole).

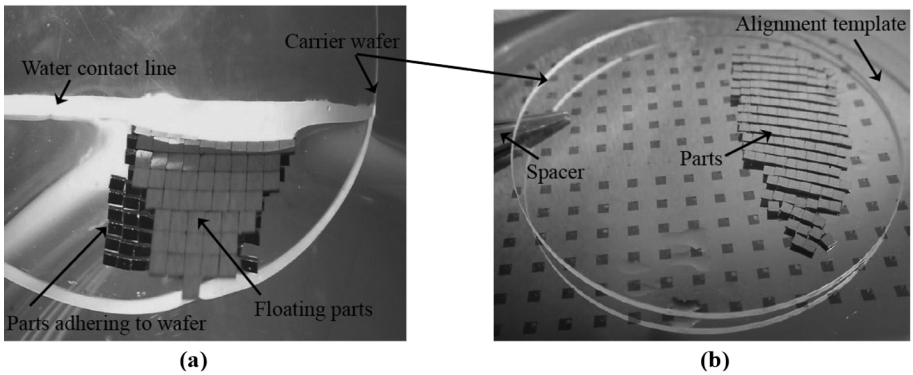

Fig. 6. The palletizing process. (a) A carrier wafer inserted into water, and floating parts adhere to the hydrophobic PFC802 surface firmly. (b) Carrier wafer brought approximately parallel to an alignment template to release the adhering parts when water evaporates.

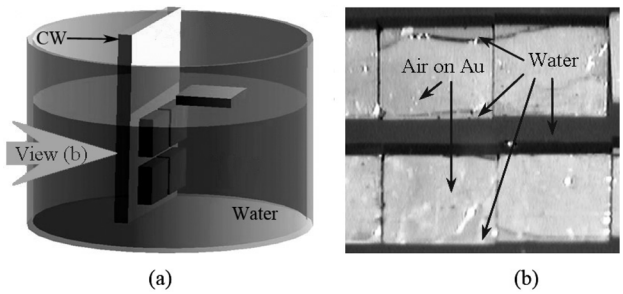

Fig. 7. Mechanism of parts adhering to the hydrophobic surface. (a) Schematic view of a carrier wafer inserted vertically into water to pick up floating parts. (b) Microscope image of trapped air bubbles underneath the parts adhering to the carrier wafer in water.

forces caused by trapped air bubbles underneath them (Fig. 7). After all the floating parts stuck to the carrier wafer, it was withdrawn completely from water, and more than 98% of the parts kept sticking to it due to capillarity of the residual water on the hydrophilic part surfaces. Finally, the carrier wafer was brought approximately parallel to the alignment template [Fig. 6(b)] on a 120 °C hotplate, and the parts were released to touch the template with their pegs when water evaporated. The carrier wafer was brought very close to the alignment template to preserve the face orientations of all the parts during the releasing.

3) Trapping Parts: We utilized orbital shaking to move the parts across the surface of the alignment template. This template was attached to an orbital shaker platform, and a Petri dish which was flipped over the template defined the moving range for all the parts. Orbital shaking can produce centrifugal forces which are evenly distributed across the shaker platform. The centrifugal forces are proportional to the square of the shaking speed and should be large enough to overcome sliding friction for the parts to move around. The 2-mm square silicon parts started to move at a shaking speed of about 150 rpm, which indicated that the sliding friction coefficient $(= \omega^2 R_s/g)$ of the alignment template was about 0.3. According to [23], a thiolated gold surface has a friction coefficient of about 0.04–0.12, which was measured by Atomic Force Microscope (AFM) tips. The friction coefficient in our experiment was greater because of several factors such as moisture or other contaminants adsorbed from the environment at the interface between the parts and the alignment template.

The moving parts were anchored by the trenches of the receptor sites. The four corner receptor sites are blocked by the Petri dish, and the remaining 164 receptor sites are open to receive parts. We performed four trapping experiments without and with 10%, 20%, 30% redundant parts (Fig. 8). During the first 10 s, the shaking speed was 200 rpm, and the trapping yield (number of occupied receptor sites/164) reached about 80% for all four cases. A slow shaking speed for the first 10 s can avoid parts flipping due to violent collisions among the crowded parts. After that, the shaking speed was raised to 250 rpm. With most of the parts anchored to the uniformly distributed receptor sites, a higher shaking speed can cause the remaining free parts to move faster to get trapped, and no part flipping was observed for all the four cases. After 3 min shaking, 95% to 99% of the receptor sites were occupied, with higher part redundancies producing higher yields.

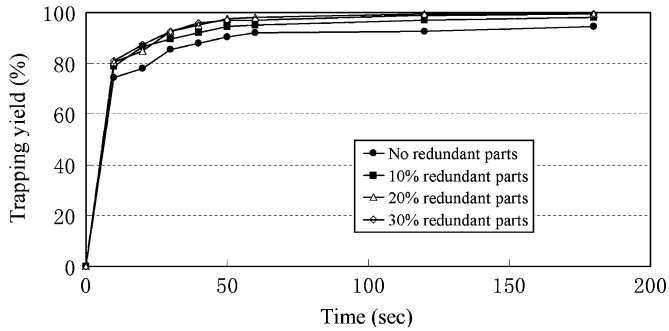

Fig. 8. Trapping results of 2-mm square silicon parts on a 164-receptor-site alignment template without and with 10–30% redundancy of parts.

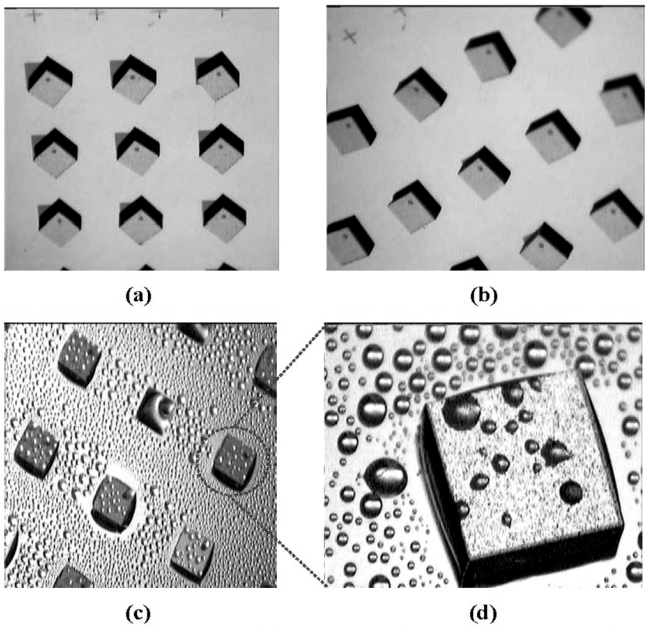

Fig. 9. Unique aligning of 2-mm square silicon parts. (a) Parts roughly aligned by gravity on a tilted alignment template. (b) Parts roughly aligned to the receptor sites on an appropriately tilted alignment template. (c) Misalignment corrected by capillary-driven self-alignment when water steam is introduced to condensate on the alignment template and parts surface. (d) Zoom view of a part with water condensate.

E. Uniquely Aligning Parts

1) Rough Alignment: We first roughly aligned the anchored parts toward a unique in-plane orientation using gravity as the driving force. On a tilted alignment template, the free parts slid away, and the anchored parts tended to rotate about their pegs until the minimum potential energy was achieved, when their centers of mass arrived at the lowest height [Fig. 9(a)-(b)]. Friction blocking the rotation of the parts was relieved with gentle knocking on the edge of the alignment template. This alignment was rough because of three factors: (1) the tilt orientation of the alignment template was roughly controlled; (2) friction from the alignment template prevented exact alignment; (3) the layout design for the parts and the receptor sites defined the exact alignment when the pegs were concentric with the trenches. The maximum translational misalignment was the difference between the radii of the circular peg and the circular trench, which was 0.25 mm. The maximum rotational misalignment we observed was about 18°.

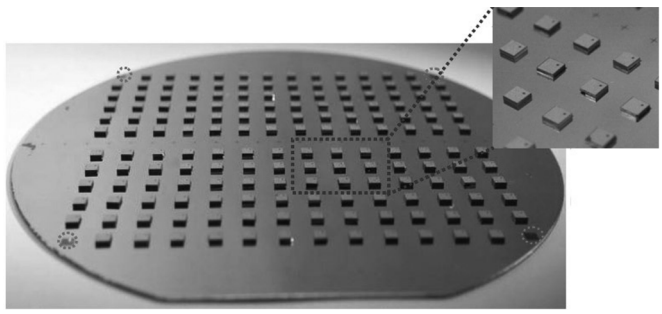

Fig. 10. The assembly result: 164 2-mm square silicon parts correctly assembled on a 4-in alignment template (the four corner receptor sites were blocked by the covering Petri dish during the trapping experiment).

2) Fine Alignment: Capillary-driven self-alignment can produce very high accuracy [15], so we introduced capillary forces to minimize the misalignment of the previous gravity-driven assembly. The alignment template with anchored parts was placed in a steam environment, i.e., a chamber having a beaker of boiling water heated by a hotplate, where water formed droplet-wise condensation on hydrophobic surfaces and film-wise condensation on hydrophilic surfaces [Fig. 9(c)–(d)]. The hydrophilic sidewall of the parts was continuously covered with water. The water on the sidewalls entered the capillary gaps between the parts and the hydrophilic receptor sites, and then lubricated the parts so that they could self-align to the receptor sites to minimize total interfacial energies. Finally, water was evaporated when the alignment template was placed on a hotplate. The final assembled array of parts is shown in Fig. 10. We observed that the misalignments from the previous rough alignment were greatly reduced: maximum rotational and translational misalignments became 3° and 50 μm, respectively.

IV. The Dry Assembly Process (DUO-SPASS)

Virtually all current assembly techniques having parallel assembly capabilities are performed in aqueous environments, e.g., fluidic shape-directed self-assembly [24], [25] and capillary-driven self-assembly [14]–[16]. In an aqueous environment, liquid flow introduces parts to receptor sites and removes unassembled parts from the assembly template. But for microchips with exposed movable microstructures, a completely dry assembly process is a better choice because these microstructures are easily stuck by surface tension of liquid residue from a wet assembly process. A completely dry assembly process is also required for microchips with materials sensitive to aqueous environments.

A. Design Rules for Alignment Features

The dry assembly process is based on two-stage shape recognition between complementary features on parts and receptor sites, and is schematically shown in Fig. 11. The first shape recognition takes places between a CP on the part and a CT on the receptor site, and the second shape recognition is accomplished between a cross peg (XP) on the part and a cross trench (XT) on the receptor site. The following design rules should be observed for appropriate two-stage shape recognition: (1) The

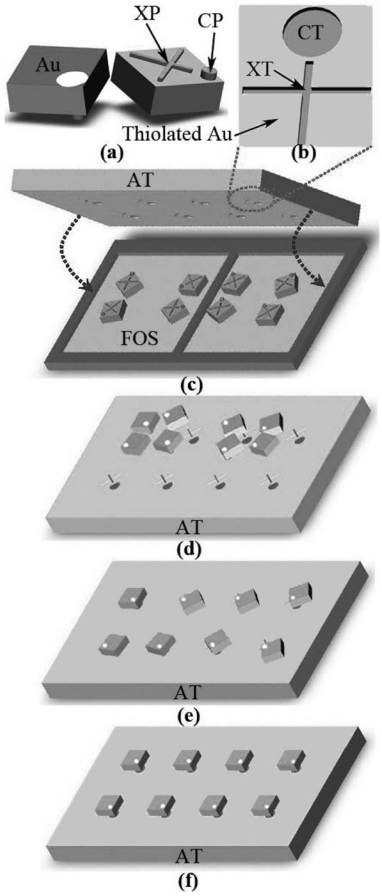

Fig. 11. Schematic overview of the DUO-SPASS process to parallel assemble square micro parts. (a) Top and bottom views of a silicon part (the bottom face has a CP and a XP, and the circular peg has twice the height of the cross peg; the top face is coated with gold, and the opening in the gold layer marks the position of the circular peg). (b) Trenches of a receptor site on the alignment template (AT). (c) Bulk parts face-oriented on an orbital shaken FOS and then sandwiched by adding an alignment template. (d) Parts palletized to the alignment template with their peg sides facing downward. (e) Parts one-to-one anchored to receptor sites by orbital shaking: the circular pegs fall into the circular trenches (first shape recognition). (f) Parts rotated by orbital shaking introduced torques until their cross pegs fall into the cross trenches (second shape recognition).

circular peg is offset from the center of mass and two times as high as the cross peg. (2) The circular trench has a greater diameter than the cross peg for fast anchoring of parts, but the circular trench diameter has an upper limit, which prevents two circular pegs of two neighboring parts or one cross peg from entering one circular trench, i.e., one circular trench is assigned exclusively to one circular peg to guarantee one-to-one registration and correct alignment. This is analogous to the condition in Section III, (1). (3) The cross trench has a greater width than the cross peg beam to anchor the cross peg quickly, but a smaller width than the diameter of the circular peg to exclude the circular peg. (4) The space between receptor sites is large enough for two neighboring parts to rotate without blocking each other and unassembled parts to slide through it. From the exact alignment layout (Fig. 12), we can determine the maximum misalignments: the maximum translational misalignment is equal to the clearance between the cross trench and cross peg, and the maximum rotational misalignment is $\tan^{-1}(2\Delta/L)$, where L is the length of the longer cross peg beam. Clearance Δ is chosen for the cross

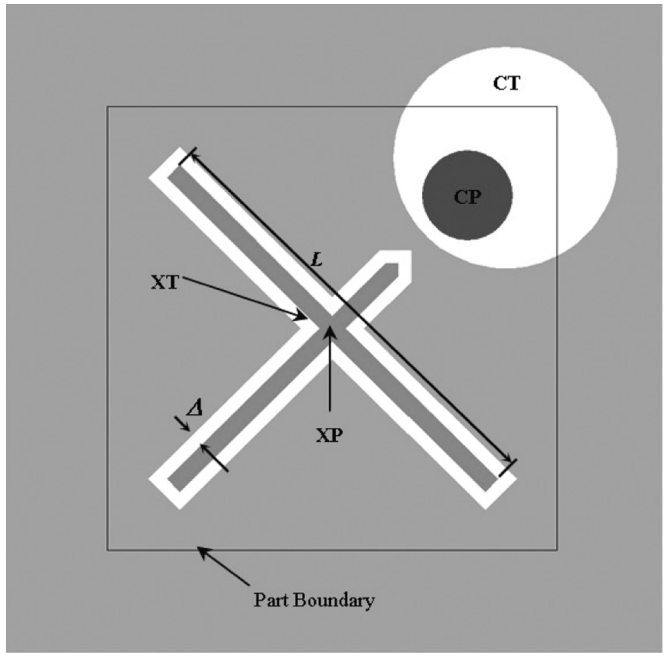

Fig. 12. A Schematic top view of the exact alignment between a part and a receptor site: the clearance Δ between the XP and XT determines maximum alignment error.

peg to enter the cross trench easily and is independent of the part size, while L can be as large as possible to obtain a minimum rotational misalignment.

B. Fabrication of Parts and the Alignment Template

1) Parts: Diced silicon parts with dimension 1 mm $\times$ 1 mm $\times$ 0.5 mm were used to demonstrate the dry assembly process. The dimension of the longer cross peg beam is 1 mm $\times$ 50 μm $\times$ 35 μm, and the diameter and height of the circular peg are 200 and 65 μm, respectively. We fabricated the circular pegs and cross pegs with different heights on a $\oslash$100 mm silicon substrate by using two subsequent DRIE processes (Fig. 13): a layer of 3900 Å thermal oxide was grown on the silicon substrate and patterned by etching to be left only on the cross peg areas, then photoresist AZ4620 was spincoated and patterned to be a DRIE mask protecting only the circular peg areas, and the patterned oxide acted as a DRIE mask with a very slow etching rate (approximately 1% of silicon etching rate) during the first DRIE and was completely removed by an oxide etchant before the second DRIE, therefore, the heights of the cross pegs and circular pegs were, respectively, determined by the first DRIE and both DRIEs. After the pegs were fabricated on the silicon substrate, we deposited a layer of TiW/Au (50/800 Å) on the backside of the silicon substrate and patterned it via double-sided lithography to form marks indicating the positions of the circular pegs.

2) Alignment Template: The recessed features for the receptor site have complementary shapes with larger dimensions for easier shape-matching: a cross trench is 40 μm greater in width than the cross peg, and the diameter of the circular trench is 300 μm greater than that of the circular peg, and both the cross trench and circular trench are 70 μm in depth. The receptor site trenches were fabricated by a single DRIE process.

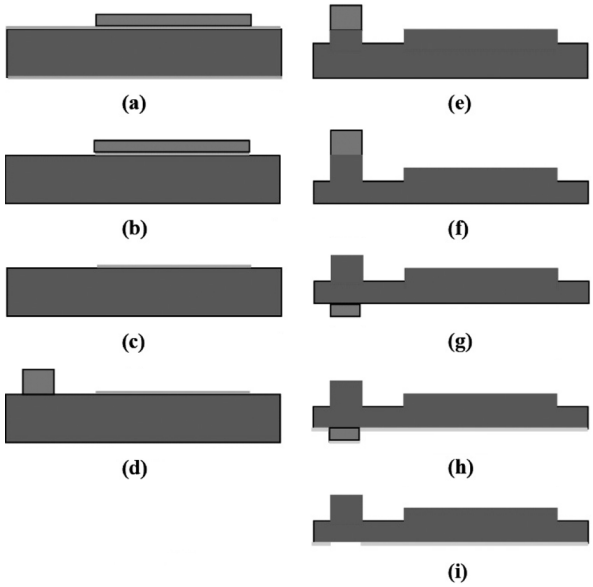

Fig. 13. Fabrication steps for the aligning features on a part with double DRIE processes. (a) AZ1512 spincoated and patterned on an oxidized silicon wafer. (b) Exposed oxide etched by BOE. (c) AZ1512 stripped. (d) AZ4620 spincoated and patterned. (e) Exposed silicon etched by DRIE. (f) Remaining oxide etched by BOE. (g) AZ4620 stripped and AZ1512 spincoated and patterned on backside of wafer. (h) Au deposited on backside. (i) AZ1512 stripped and Au on top of it lifted off.

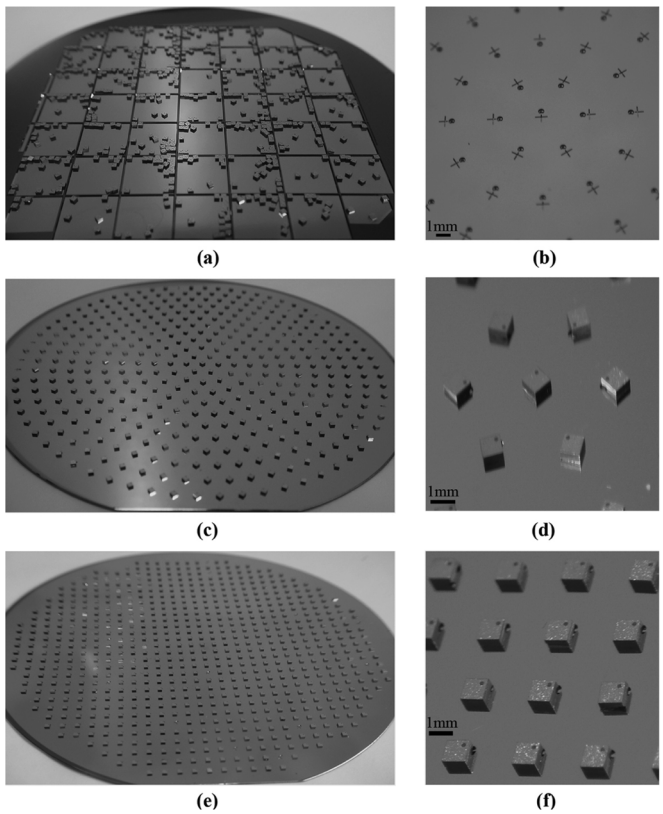

Fig. 14. Optical photographs of templates and assembly results. (a) After 1 min of orbital shaking, only four silicon parts stay tilted by their pegs on the ⌀100-mm FOS. (b) A partial view of an alignment template with a polar array of receptor sites. (c) 388 silicon parts assembled on the ⌀100 mm alignment template with a polar array of 397 receptor sites. (d) Zoom-in view of the center of the alignment template. (e) 710 silicon parts assembled on the ⌀100 mm alignment template with an orthogonal array of 720 receptor sites. (f) Zoom-in view of a 4 × 3 section of the array of receptor sites.

We fabricated two ⌀100 mm alignment templates, respectively, having a polar/orthogonal array of 397/720 receptor sites. For simplicity, we describe the complete assembly process only for the polar 397-receptor-site alignment template.

To reduce sliding friction of the silicon alignment template, we deposited a layer of TiW/Au (50/800Å) and soaked the alignment template in a 1-mmol alkanethiol $CH_3(CH_2)_{11}SH$ (in ethanol) solution overnight for the Au surface to adsorb a SAM. The thiolated gold surface has a lower friction coefficient than that of a silicon surface, so that less agitation is required to move parts on the alignment template.

C. Uniquely Face-Orienting Bulk Parts

On an orbitally shaken substrate, the silicon part can not rest on its face with alignment pegs in a stable way, because the part is tilted by its cross peg and easily flipped by the centrifugal force introduced by orbital shaking. Initially bulk silicon parts were stored in a container with random face orientations. We used orbital shaking to orient all the parts to face the same direction with their pegs on a substrate.

A face-orienting substrate (FOS) has an array of trenches, which confine parts locally. We fabricated this substrate out of an oxidized ⌀100 mm silicon substrate with TAMH etching: oxide was first patterned to produce the silicon etching mask, and 4 h etching at 90 °C resulted in 240-μm deep trenches.

Bulk silicon parts were uniquely face-oriented on a FOS by orbital shaking. 600 parts (about 50% redundant parts aiming for a high assembly yield) were poured with an approximately uniform distribution onto a FOS attached to the platform of an orbital shaker. Then the shaker ran at 200 rpm for about 1 min and its centrifugal force flipped over all but four tilted parts onto their flat faces, while all the other parts stayed resting on their flat faces [Fig. 14(a)]. All the remaining four tilted parts had been kept immobile by surrounding parts. In order to face-orient bulk parts and keep them locally confined, the orbital shaker needs to be run within a narrow speed range of about 50 rpm: a speed higher than 230 rpm can cause parts moving across the FOS and parts tend to be crowded into a few substrate trenches, and a speed lower than 180 rpm cannot flip the tilted parts[1]. The upper speed limit is determined by the trench depth. The lower speed limit depends on the part tilt angle or the ratio between the peg height and the part side length. The parts' "preference" not to rest on their peg sides is due to the higher centers of gravity in this position and the higher friction at the off-center peg tips, which in combination cause larger torques during orbital shaking.

D. Palletizing Parts

We placed the alignment template [Fig. 14(b)] with its receptor sites facing the FOS to sandwich the parts, and turned them over. Thereby, the patterned ridges on the substrate kept the parts in place. Then we removed the substrate, and 99% of the parts were transferred to the alignment template except very few parts sticking to the FOS due to adhesive forces.

[1]This bound is lower than that in Section III-E (>250 rpm) because here parts are smaller (1 mm) with taller pegs, and, thus, are less stable to rest on their pegs.

E. The Assembly Process

We utilized a mechanism based on two-stage shape recognition to assemble the palletized parts. The alignment template surface coated with thiolated Au has less sliding friction than a silicon surface, and to reduce friction effects even further, we attached the alignment template to an ultrasonic stage mounted on an orbital shaker. To move the parts around without flipping over, the orbital shaker was run in a speed range whose limits were given as follows: the lower speed limit introduced a centrifugal force just enough to overcome the friction; the upper speed limit caused the tilted parts to flip over. We ran the orbital shaker at 110 rpm[2]. The moving parts were first anchored to the receptor sites when their circular pegs fell into the circular trenches, and came to rest horizontally on their cross pegs. Because the circular pegs were offset from the center of mass, the centrifugal force from orbital shaking exerted torques on the anchored parts to drive them to rotate about their circular pegs until their cross pegs fell into the cross trenches; at this point the parts were fixed to the uniquely defined orientations. After 10 min agitation, 388 receptor sites were correctly registered with parts, which indicated a yield of 97.7% [Fig. 14(c)-(d)]. We removed the unassembled parts from the alignment template by tilting the ultrasonic stage so that gravity drove them to slide away.

We also assembled the same silicon parts on a $\oslash$100 mm alignment template with 720 receptor sites according to the above process steps. 50% redundant parts were used. 710 parts were correctly assembled within 10 min, i.e., the assembly yield reached 98.6% [Fig. 14(e)–(f)].

The maximum alignment errors are determined by the design of the complementary features on the parts and the receptor sites. The maximum translational misalignment is equal to the clearance Δ between the cross peg and the cross trench, which is 20 μm in our design. The maximum rotational misalignment is about 2°.

F. Assembly Defects

During the assembly process, we noticed two major types of defects: 1) occasionally unassembled parts adhered to the assembled parts; 2) parts resting on their flat faces were immobile during the agitation, which blocked other moving parts. The part sticking was mainly caused by contamination from the previous process steps. Because the face-orienting process did not have perfect 100% yield, some parts rested on their flat faces after palletizing. We manually removed these parts to avoid the second type of defects. In addition, we kept the vibration intensity of the ultrasonic stage low enough to prevent parts from flipping over.

V. Wafer Level Flip-Chip Bonding

In this paper, we focus on a novel approach for palletizing and assembling of parts using uniquely orienting self-assembly, so that we used dummy silicon parts without any functional circuit or interconnect pad to demonstrate all the previous process steps. As for the final step of our packaging strategy, we propose a wafer-level flip-chip bonding technique to package functional microchips onto a CCT. The flip-chip bonding can be achieved via solder bumps deposited on a chip carrier template [Fig. 1(f)] or a layer of anisotropic conductive film [26], as currently done in well-established industrial IC packaging processes.

[2]This speed is lower than that in Section III.E mainly because here an ultrasonic vibration stage is used to reduce sliding friction.

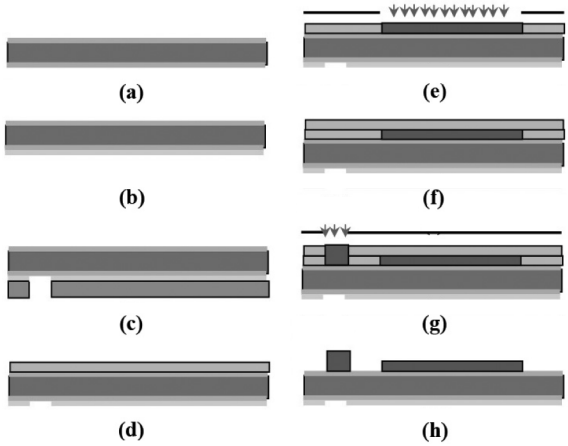

Fig. 15. Fabrication steps for the aligning features on a part with double layers of SU8. (a) LPCVD nitride deposited on the silicon wafer. (b) Au deposited on backside of wafer. (c) AZ1512 is photolithographically patterned on Au to expose peg marker areas and Au etched in an Au etchant. (d) A layer of SU8 spincoated on the front side. (e) SU8 exposed to UV light with a mask protecting the areas other than cross-alignment pegs. (f) Second layer of SU8 spincoated. (g) SU8 in the circular peg areas exposed to UV light. (h) SU8 developed.

VI. Application to Non-Silicon Parts

Both the semi-DUO-SPASS and DUO-SPASS assembly processes can be also applicable to parts made of nonsilicon materials, when combined with additive fabrication techniques for the pegs on the parts. For the semidry process, the single circular peg can be easily fabricated with a single SU8 casting process. For the dry process, we fabricated two high-aspect-ratio pegs on each part with different heights out of the photodefinable polymer SU8-2025 (MicroChem Corporation, MA) with the following major fabrication process steps (Fig. 15): 1) first layer of SU8 was spincoated and UV light exposed with a mask having transparent areas for cross pegs; 2) second layer of SU8 was spincoated and UV light exposed with a mask having transparent areas for circular pegs; 3) SU8 was developed, and then only the circular pegs and cross pegs exposed by UV light were left on the substrate. An array of SU8 pegs is shown in Fig. 16. During the assembly of the parts with SU8 pegs (also 50% redundant parts provided) on the previous 397-receptor-site alignment template, we obtained a lower yield (about 80%) within longer time (half an hour) than the parts with silicon pegs, which is mainly because SU8 has a greater friction coefficient than silicon.

VII. Conclusion and Discussions

We have presented a wafer-level packaging strategy for micro device chips based on uniquely orienting self-assembly, and demonstrated semidry assembly of 2-mm square silicon parts and completely dry assembly of 1 mm square silicon parts on 4-in alignment templates. Both assembly processes have yields close to 100%. Our assembly strategy can also be applied to flat

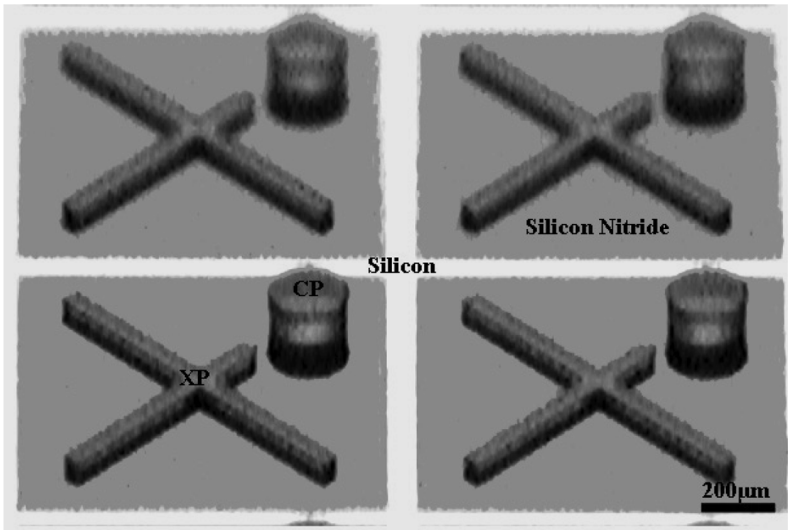

Fig. 16. An optical microscope image of a 2 × 2 section of an array with SU8-2025 CP and XP on a 3-inch silicon substrate, before dicing into individual parts.

parts of any shape with a larger or smaller scale if the alignment feature design rules are observed. Adhesive and friction forces, which are the major causes for potential failures of our assembly techniques, become more significant compared with gravitational forces for smaller parts. Our assembly method has been demonstrated with 1- and 2-mm square parts, and we believe that it can assemble larger device chips with dimension up to centimeters which are less affected by adhesive forces. In micro domains, both the adhesive and frictional forces are approximately proportional to contact area. The adhesive forces come mainly from electrostatic interactions, van der Waals attractive forces and surface tension from adsorbed moisture on the part and the substrate [27]. The gold face of the alignment template can eliminate the electrostatic charges at the bottom faces of parts, but not the charges at the sidewalls of parts, which can cause parts sticking to each other. A photoionizer can effectively neutralize electrostatic charges on any exposed surface by introducing ions into the surrounding atmosphere. Adsorbed moisture can be reduced by heating the alignment template or performing the assembly in a vacuum environment. With good control of environment humidity, electrostatic charges and sliding friction, we believe that our assembly process can handle parts of much smaller size.

An accurate model for the friction and stiction forces at the part edges and peg tips would be valuable for design optimization. A systematic approach would study the balance between these stiction forces and the orbital shaker-induced torque that causes part flipping. Parts with minimal peg heights may be desired because of manufacturing constraints.

Peg height is a key factor for proper assembly of parts in both assembly processes: 1) a minimum height of the circular peg is required for reliable anchoring of parts: $\sim$20 μm for the semi-DUO-SPASS process, $\sim$30 μm higher than the cross peg for the DUO-SPASS process due to ultrasonic vibration to relieve sliding friction; 2) minimum orbital shaking speeds to move and flip over parts (denoted as ω_m and ω_f) depend on the part/substrate contact area and the ratio between height of the circular peg and side length of the part, respectively.

In our experiments we continuously monitored the progress of the assembly, but the goal is to run these processes completely open-loop. We believe that in an industrial setting, simply following a timed recipe will suffice (see Fig. 8 with the trapping yield as a function of time). But expecting 100% yield may be unrealistic for large assemblies, and an automated vision system with a precision robot could be used to fix the few remaining defects.

Our packaging mechanism itself applies no upper limit on the alignment template size. All the agitations required in the assembly process are orbital shaking, which introduces centrifugal forces evenly distributed all across the shaker platform. The orbital shaker platform supported by three rotating arms can be easily expanded. High-aspect-ratio trench features on the alignment template can be fabricated with many available techniques such as DRIE (only for silicon templates), molding, and others [28]–[30]. These trench fabrication techniques limit the alignment template size.

In addition to wafer-level packaging of micro device chips, our assembly techniques without the final bonding step can also be used as part feeding and palletizing for robotic assembly systems.

ACKNOWLEDGMENT

The authors would like to thank the group members of the MEMS Laboratory, University of Washington, Seattle, for helpful comments and discussions, and staff of the Washington Technology Center Microfabrication laboratory for their help and support. The generous hospitality during K. Böhringer's stay at the laboratories of Prof. M. Esashi (Tohoku University), Prof. H. Fujita, Prof. S. Takeuchi (University of Tokyo), and Prof. O. Tabata (University of Kyoto) was greatly appreciated.

REFERENCES

[1] M. B. Cohn, K. F. Böhringer, J. M. Noworolski, A. Singh, C. G. Keller, K. Y. Goldberg, and R. T. Howe, "Microassembly technologies for mems," in *Proc. SPIE Micromach. Microfabricat.*, Santa Clara, CA, Sep. 1998, pp. 2–16.

[2] S. J. Ralis, B. Vikramaditya, and B. J. Nelson, "Micropositioning of a weakly calibrated microassembly system using coarse-to-finestrategies," *IEEE Trans. Electron. Packag. Manuf.*, vol. 23, pp. 123–131, 2000.
[3] C.-T. Su and H. P. Fu, "A simulated annealing heuristic for robotics assembly using the dynamic pick-and-place model," *Prod. Plann. Control*, vol. 9, pp. 795–802, 1998.
[4] J. A. Thompson and R. S. Fearing, "Automating microassembly with ortho-tweezers and force sensing," in *Proc. IROS2001*, Maui, HI, 2001, pp. 1327–1334.
[5] A. Würsch and M. Scussat, "An innovative micro optical elements assembly robot characterized by high accuracy and flexibility," in *Proc. ECTC2000, PAPER 41*, Las Vegas, NV, 2000.
[6] G. Yang, J. A. Gaines, and B. J. Nelson, "A flexible experimental workcell for efficient and reliable wafer-level 3d microassembly," in *Proc. ICRA2001*, Seoul, South Korea, 2001, pp. 133–138.
[7] K. P. Ellis, F. J. Vittes, and J. E. Kobza, "Optimizing the performance of a surface mount placement machine," *IEEE Trans. Electron. Packag. Manuf.*, vol. 24, pp. 160–170, 2001.
[8] M. B. Cohn, Y. C. Liang, R. T. Howe, and A. P. Pisano, "Wafer-to-wafer transfer of microstructures for vacuum packaging," in *Proc. Solid-State Sens. Actuator Workshop*, Hilton Head Island, SC.
[9] A. S. Holmes and S. M. Saidam, "Sacrificial layer process with laser-driven release for batch assembly operations," *J. Microelectromech. Syst.*, vol. 7, pp. 416–422, 1998.
[10] D. S.-W. Park, K. Kim, B. Pillans, and J.-B. Lee, "Polydimethylsiloxanebased pattern transfer process for the post-ic integration of mems onto cmos chips," *J. Micromech. Microeng.*, vol. 14, pp. 335–340, 2004.
[11] A. Singh, D. A. Horsley, M. B. Cohn, A. P. Pisano, and R. T. Howe, "Batch transfer of microstructures using flip-chip solder bonding," *J. Microelectromech. Syst.*, vol. 8, pp. 27–33, 1999.
[12] H. J. Yeh and J. S. Smith, "Fluidic self-assembly for the integration of gaas light-emitting diodes on si substrates," *IEEE Photon. Technol. Lett.*, vol. 6, pp. 706–708, 1994.
[13] W. Zheng, P. Buhlmann, and H. O. Jacobs, "Sequential shape-and-solderdirected self-assembly of functional microsystems," in *Proc. Nat. Acad. Sci.*, 2004.
[14] H. O. Jacobs, A. R. Tao, A. Schwartz, D. H. Gracias, and G. M. Whitesides, "Fabrication of cylindrical display by patterned assembly," *Science*, vol. 296, pp. 323–325, 2002.
[15] U. Srinivasan, D. Liepmann, and R. T. Howe, "Microstructure to substrate self-assembly using capillary forces," *J. Microelectromech. Syst.*, vol. 10, pp. 17–24, 2001.
[16] J. Fang, K. Wang, and K. F. Böhringer, "Self-assembly of micro pumps with high uniformity in performance," in *Proc. Solid State Sens., Actuator, and Microsystems Workshop*, Hilton Head Island, SC, 2004.
[17] L. F. Miller, "Controlled collapse reflow chip joining," *IBM J. Res. Dev.*, vol. 13, pp. 239–250, 1969.
[18] L. S. Goodman, "Geometric optimization of controlled collapse interconnections," *IBM J. Res. Dev.*, vol. 13, pp. 251–265, 1969.
[19] G. Boothroyd, C. Poli, and L. E. Murch, *Automatic Assembly*, G. Boothroyd, C. Poli, and L. Murch, Eds: Marcel Dekker, Inc., 1982.
[20] K. F. Böhringer, B. R. Donald, and N. C. Macdonald, "Programmable vector fields for distributed manipulation, with applications to mems actuator arrays and vibratory parts feeders," *Int. J. Robot. Res.*, vol. 18, pp. 168–200, 1999.
[21] S. Sorensen and R. Stringham, "Feature vision guided flexible feeding made easy," *Indust. Robot*, vol. 26, pp. 99–104, 1999.
[22] R. L. Bayt, K. S. Breuer, and A. A. Ayon, "Drie-fabricated nozzles for generating supersonic flows in micropropulsion systems," in *Proc. Solid State Sens., Actuator, and Microsystems Workshop*, Hilton Head Island, SC, 1998.
[23] S. Jiang, "Molecular simulation studies of self-assembled monolayers of alkanethiols on Au(111)," *Molec. Phys.*, vol. 100, pp. 2261–2275, 2002.
[24] J. S. Smith and J. Yeh, "Method and apparatus for fabricating self-assembling microstructures," U.S. Patent 5 824 186, 1998.
[25] J. S. Smith and J. Yeh, "Apparatus for fabricating self-assembling microstructures," U.S. Patent 5 904 545, 1999.
[26] Anisotropic conductive film for flipchip applications: An introduction, P. J. Opdahl. [Online]. Available: http://www.flipchips.com/tutorial05.htm
[27] R. S. Fearing, "Survey of sticking effects for micro parts," in *Proc. IROS95*, Pittsburgh, PA, Aug. 1995.
[28] M. D. B. Charlton and G. J. Parker, "Fabrication of high aspect ratio silicon microstructures by anodic etching," *J. Micromech. Microeng.*, vol. 7, pp. 155–158, 1997.
[29] K. Kim, S. Park, J.-B. Lee, H. Manohara, Y. Desta, M. Murphy, and C. H. Ahn, "Rapid replication of polymeric and metallic high aspect ratio microstructures using pdms and liga technology," *Microsyst. Tech.*, vol. 9, pp. 5–10, 2002.
[30] Y. Zhao and T. Cui, "Fabrication of high-aspect-ratio polymer-based electrostatic comb drives using the hot embossing technique," *J. Micromech. Microeng.*, vol. 13, pp. 430–435, 2003.

Jiandong Fang received the Bachelor's degree in physics from the University of Science and Technology of China in 1999, and the Master's degree in physics from the University of Washington, Seattle, in 2001. He is currently a Ph.D. degree candidate in the Department of Electrical Engineering, University of Washington.

His research interests include micro fluidic systems, microoptical systems, self-assembly processes, and massively parallel packaging of micro devices.

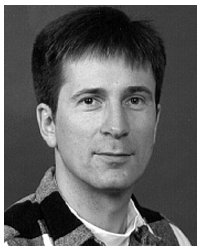

Karl F. Böhringer (S'94–M'97–SM'03) received the Dipl.-Inform. degree from the University of Karlsruhe, Germany, in 1990 and the M.S. and Ph.D. degrees in computer science from Cornell University, Ithaca, NY, in 1993 and 1997, respectively.

He was a Visiting Scholar with Stanford University, Stanford, CA, during 1994–1995 and a Postdoctoral Researcher with the University of California, Berkeley, from 1996 to 1998. He joined the Electrical Engineering Department, University of Washington, Seattle, in 1998, where he is currently an Associate Professor. He also held visiting faculty positions with the Universities of Tohoku, Tokyo, Kyoto, Japan, and São Paulo, Brazil. His research interests include microelectromechanical systems (MEMS), manipulation and assembly from macro to nano scales, microfluidic systems for the life sciences, and microrobotics. He has created, among others, multibatch self-assembling systems, massively parallel microactuator arrays, and a walking microrobot.

Dr. Böhringer is member of the Society for Nanoscale Science, Computing and Engineering (ISNSCE), the American Society for Engineering Education (ASEE), and the German Society for Information Sciences (GI). He was awarded a Long-Term Invitational Fellowship for Research in Japan by the Japan Society for the Promotion of Science (JSPS) in 2004, an IEEE Robotics and Automation Society Academic Early Career Award in 2004, an NSF CAREER Award in 1999, and an NSF Postdoctoral Associateship in 1997. His work was listed among the "Top 100 Science Stories of 2002" in *Discover* magazine. He is an Associate Editor of the ASME/IEEE JOURNAL OF MICROELECTROMECHANICAL SYSTEMS and the IEEE TRANSACTIONS ON AUTOMATION SCIENCE AND ENGINEERING and has served on technical program committees for the IEEE MEMS and Transducers conferences.